ENVIRONMENTAL RESEARCH
LETTERS

LETTER • OPEN ACCESS

An evaluation of advanced baseline imager fire radiative power based wildfire emissions using carbon monoxide observed by the Tropospheric Monitoring Instrument across the conterminous United States

To cite this article: Fangjun Li *et al* 2020 *Environ. Res. Lett.* **15** 094049

Environmental Research Letters

LETTER

An evaluation of advanced baseline imager fire radiative power based wildfire emissions using carbon monoxide observed by the Tropospheric Monitoring Instrument across the conterminous United States

Fangjun Li[1], **Xiaoyang Zhang**[1], **Shobha Kondragunta**[2] **and Xiaoman Lu**[1]

[1] Geospatial Sciences Center of Excellence, Department of Geography and Geospatial Sciences, South Dakota State University, Brookings, SD 57007, United States of America
[2] NOAA/NESDIS/Center for Satellite Applications and Research, College Park, MD 20740, United States of America

E-mail: fangjun.li@sdstate.edu

Keywords: fire radiative power, GOES-16, TROPOMI, carbon monoxide, wildfire, fire emissions

OPEN ACCESS

RECEIVED
14 April 2020

REVISED
27 May 2020

ACCEPTED FOR PUBLICATION
16 June 2020

PUBLISHED
24 August 2020

Abstract

Biomass-burning emissions (BBE) profoundly affect climate and air quality. BBE have been estimated using various methods, including satellite-based fire radiative power (FRP). However, BBE estimates show very large variability and the accuracy of emissions estimation is poorly understood due to the lack of good reference data. We evaluated fire emissions estimated using FRP from the Advanced Baseline Imager (ABI) on GOES-R (Geostationary Operational Environmental Satellites-R) by comparing with the Sentinel 5 Precursor TROPOspheric Monitoring Instrument (TROPOMI) Carbon Monoxide (CO) over 41 wildfires across the United States during July 2018—October 2019. All the ABI FRP-based CO and TROPOMI CO emissions were significantly correlated and showed a very good agreement with a coefficient of determination of 0.94 and an accuracy of 13–18%. We further reported a CO emission coefficient of 29.92 $\pm$ 2.39 g MJ^{-1} based on ABI FRP and TROPOMI CO, which can be used to directly estimate BBE from FRP observed from satellites. Based on the CO emission coefficient and ABI FRP, we finally estimated a monthly mean CO of 596 Gg across the Conterminous United States for June—September 2018.

1. Introduction

Global fires emit a very large amount of trace gases and aerosols that significantly influence climate (Tosca *et al* 2013) and degrade air quality (Johnston *et al* 2012). Biomass-Burning Emissions (BBE) have been estimated conventionally using knowledge of burned area, fuel loads, combustion coefficient, and emission factors since the 1980s (Seiler and Crutzen 1980, van der Werf *et al* 2017). Yet large uncertainties in these parameters limit the accuracy of emissions estimation (Randerson *et al* 2012). For instance, burned area from MODIS (Moderate Resolution Imaging Spectroradiometer), which has been widely used in conventional emission inventories, is underestimated by up to 80% in Africa compared with the Landsat-8 and Sentinel-2 based burned area (Roteta *et al* 2019, Roy *et al* 2019). BBE have also been estimated using inverse modeling by constraining chemical transport models (CTMs) with satellite observations of certain emissions species [e.g. carbon monoxide (CO) from Measurements Of Pollution In The Troposphere (MOPITT)] (Heald *et al* 2004, Shindell *et al* 2006, Duncan *et al* 2007, Jones *et al* 2009, Kopacz *et al* 2010, Jiang *et al* 2017). The inverse modeling and CTMs involve the configuration of many physical, chemical, and meteorological variables and generally make assumptions of biases and uncertainties in these variables (Shindell *et al* 2006, Duncan *et al* 2007). Because different assumptions could lead to significant systematic errors of inverse models (Heald *et al* 2004, Shindell *et al* 2006), the accuracy of BBE estimation could be influenced by >20% globally (Jiang *et al* 2011, 2013) and >80% regionally (Jiang *et al* 2013).

Fire radiative power (FRP), the instantaneous radiative energy emitted from fire, has been shown to be a reliable method to estimate BBE. Lab and small-scale field experiments have demonstrated that FRP can be empirically related to biomass combustion rate via combustion factor (Wooster

et al 2005, Freeborn et al 2008) and smoke emissions rate via emission coefficient (Ichoku and Kaufman 2005, Freeborn et al 2008, Ichoku et al 2008), which has been further confirmed in landscape wildfires (Kremens et al 2012, Li et al 2018, Mota and Wooster 2018, Lu et al 2019). These empirical relationships enable direct calculation of the amount of consumed biomass or emitted emissions during a fire event using temporally integrated FRP (termed fire radiative energy or FRE) observed from satellites. Although satellite-based FRP has been increasingly used to estimate regional-to-global fire emissions in the past decade (Vermote et al 2009, Kaiser et al 2012, Zhang et al 2012, Ichoku and Ellison 2014, Darmenov and da Silva 2015, Roberts et al 2015, Mota and Wooster 2018, Li et al 2019), the parameters that convert FRP to BBE differ significantly among different studies and the widely used FRP observations from polar-orbiting sensors (e.g. MODIS) are not able to characterize the diurnal variation of fires that is a crucial element of computing BBE. As a result, BBE estimates in different products vary by a factor of up to 10 (Zhang et al 2014a, Li et al 2019, Carter et al 2020). The accuracy of BBE is usually assessed by applying BBE to predict aerosol optical depth (AOD) using CTMs and then comparing the model predicted AOD with independent observations such as ground-based sunphotometer measurements or satellite-derived AOD (Zhang et al 2014a, Carter et al 2020). Similarly, BBE estimates are also evaluated using trace gases such as CO or carbon oxide (CO2) from other independent observations (Pechony et al 2013, Huijnen et al 2016, Heymann et al 2017, Dekker et al 2019). However, this evaluation approach is significantly limited by uncertainties in the model prediction of AOD (Curci et al 2015, Das et al 2017) and concentrations of trace gases (Jiang et al 2011, 2013). Therefore, full validation of the FRP-based BBE is critical but remains challenging. This is primarily due to the lack of high-quality measurements of fire emissions as a reference on a large scale.

Here we propose a new approach to evaluate the FRP-based BBE and derive smoke emission coefficient using observations at relatively fine spatiotemporal resolutions from two new satellite instruments: the Advanced Baseline Imager (ABI) on the latest GOES-R (Geostationary Operational Environmental Satellites—R Series) and the TROPOspheric Monitor Instrument (TROPOMI) on the Copernicus Sentinel 5 Precursor (Sentinel-5P). Specifically, we selected 41 wildfires with isolated fresh smoke plumes across the Conterminous United States (CONUS) during July 2018—October 2019. The FRE and BBE for each wildfire were calculated from the 2-km ABI observations every 5 min and the total mass of fire CO emissions was directly obtained from the 7-km TROPOMI CO data. Then, the ABI FRP-based BBE was evaluated using TROPOMI CO and the CO emission coefficient was further derived based on TROPOMI CO and ABI FRE. Finally, the derived CO emission coefficient and ABI FRP were used to estimate the CO emissions across the CONUS, which were compared with three satellite active fire data based BBE inventories: the Fire Inventory from NCAR (FINN), the Global Fire Assimilation System (GFAS), and the Quick Fire Emissions Dataset (QFED).

2. Data

2.1. GOES-16 ABI FRP

The GOES-R ABI detects fires at a nominal spatial resolution of 2 km (at nadir). GOES-16, the first GOES-R satellite positioned at 75.2° W, has been operationally running since December 2017. GOES-16 ABI scans the CONUS every 5 min with a pixel area increasing from 4.8–16.8 km^2 as satellite view zenith angle (VZA) varies from 29–72°. GOES-16 ABI detects fires using the 3.9-μm and 11.2-μm bands and provides for each fire pixel the detection time, geolocation, fire temperature, fire area, FRP (MW per pixel), and fire mask quality flag (Schmidt et al 2013). FRP is calculated using radiances of a fire pixel and its ambient background non-fire pixels in the 3.9-μm band (Schmidt et al 2013). The fire detection performance of GOES-16 ABI has been evaluated using the 30-m Landsat-8 and 375-m VIIRS (the Visible Infrared Imaging Radiometer Suite) active fire data and ground fire records (Hall et al 2019, Li et al 2020), which shows that GOES-16 ABI is able to confidently detect fires with FRP >34.5 MW (Li et al 2020). Compared with the 750-m VIIRS FRP, GOES-16 ABI FRP is relatively larger in individual fires but generally comparable at a regional scale across the southeastern CONUS (Li et al 2020). This study obtained GOES-16 ABI active fire data during July 2018—October 2019 from NOAA Comprehensive Large Array-data Stewardship System (CLASS) (https://www.avl.class.noaa.gov/; last accessed on 3 April 2020).

2.2. Sentinel-5P TROPOMI CO and aerosol index

Sentinel-5P TROPOMI observes global CO at a nominal spatial resolution of 7 km. Sentinel-5P crosses the equator at ~13:35. TROPOMI senses earth reflected radiances over a scan angle range of ±54° with a swath width of ~2600 km (Veefkind et al 2012). TROPOMI CO is retrieved using radiances in the shortwave infrared bands (SWIR, 2305–2385 nm) based on the Shortwave Infrared CO Retrieval (SICOR) algorithm (Vidot et al 2012, Landgraf et al 2016). The ground pixel size of SWIR bands is generally consistent (7 km) in the along-track direction but varies from 7 km at nadir to 34 km at the scan edge in the across-track direction (Veefkind et al 2012). The 7-km TROPOMI Level 2 CO product provides for each pixel observation time, coordinates (longitude and latitude), satellite VZA, solar zenith angle, CO

total column density (mol m^{-2}), and retrieval precision. The vertical sensitivity of the CO total column density retrievals depends on the total column averaging kernels that are sensitive to clouds (Borsdorff *et al* 2018a). The averaging kernel of the CO total column density across the globe in clear-sky conditions has been demonstrated to be close to 1.0 at all altitudes, which suggests that the CO total column retrievals represent the true CO total columns very well (Borsdorff *et al* 2018a). The validation also shows that TROPOMI CO data agree with ground-based CO observations and model-simulated CO data well (Borsdorff *et al* 2018b, 2018c).

The TROPOMI sensor also senses aerosols using the ultraviolet bands (UV). The ground pixel size of TROPOMI UV bands is 7 km in the along-track direction and varies from 3.5 km at nadir to 15 km at the scan edge in the cross-track direction, which is ∼2 times finer than the SWIR bands (Veefkind *et al* 2012). The TROPOMI Level 2 aerosol index (AI) product calculates AI based on the 354/388 nm and 340/380 nm pair bands (Apituley *et al* 2018). A positive AI indicates the presence of absorbing aerosols (i.e. smoke from fires, and volcanic ash, and dust). Thus, this study obtained the TROPOMI Level 2 CO and AI products for the period from July 2018–October 2019 from the Copernicus Sentinel-5P pre-operations data hub (https://s5phub.copernicus.eu/; last accessed on 3 April 2020).

2.3. Terra MODIS and S-NPP VIIRS true-color imageries

The true-color (RGB) images from Terra MODIS and VIIRS onboard S-NPP (the Suomi National Polar-Orbiting Partnership) are obtained to identify visually interpretable fresh smoke plumes. The daily global true-color composites based on MODIS and VIIRS surface reflectance are available on the NASA (National Aeronautics and Space Administration) Worldview tool (https://worldview.earthdata.nasa.gov/).

2.4. Three BBE inventories

The FINN, GFAS, and QFED emissions inventories provide daily global fire emissions, including CO, based on the 1-km MODIS active fire data (Wiedinmyer *et al* 2011, Kaiser *et al* 2012, Darmenov and da Silva 2015). The FINN inventory estimates emissions at the fire pixel level using the conventional bottom-up method, with the parameters-burned area and fuel consumption calculated in each MODIS fire detection (Wiedinmyer *et al* 2011). The GFAS calculates emissions using MODIS FRP and the land cover specific FRE combustion factors that are derived by relating MODIS FRP to the dry matter combustion ratio from the Global Fire Emission Database (GFED3.1) (Kaiser *et al* 2012). The QFED estimates emissions using MODIS FRP and emission coefficients that are derived in two steps: first obtain initial factors by relating MODIS FRP to GFED emissions in four biomes, and then adjust the initial factors by comparing the model-simulated AOD with MODIS AOD (Darmenov and da Silva 2015). This study obtained the FINN v1.5 (http://bai.acom.ucar.edu/Data/fire/; last accessed on 18 May 2020), the GFAS v1.2 (https://apps.ecmwf.int/datasets/data/cams-gfas/; last accessed on 18 May 2020), and the QFED v2.5r1 (https://portal.nccs.nasa.gov/datashare/iesa/aerosol/emissions/QFED/v2.5r1/0.1/; last accessed on 18 May 2020) emissions data for the period from June to September 2018.

3. Methods

3.1. Selection of fire events with fresh smoke plumes

Fire events with fresh smoke plumes were selected based on active fire data from GOES-16 ABI and natural color imageries from both Terra MODIS and S-NPP VIIRS. Specifically, the ABI fire detections with valid FRP were first used to locate potential fire events. Then for each fire event the VIIRS natural color reflectance composite was employed to examine if the fire released any visually interpretable smoke plumes that contrast sharply with background and are not contaminated by clouds and smoke from other fire events. Meanwhile, Terra MODIS natural color reflectance was used to determine the age of smoke plumes. In this study, we define that a smoke plume is fresh if it is released within a few hours (i.e., 3 h) of TROPOMI overpass. Because Terra MODIS overpasses (10:30) the same area ∼3 h earlier than S-NPP VIIRS (13:30) and Sentinel-5P TROPOMI (13:35), a fire event is selected if the Terra MODIS reflectance composite shows no smoke plumes (or smoke with very limited size) associated with the fire but VIIRS reflectance shows very clear smoke plumes. Figures 1(a)–(f) shows the selection process of two fires in northern Colorado on 22 September 2018, where the associated two smoke plumes released after Terra MODIS overpass were observed by S-NPP VIIRS and further confirmed by ABI active fire detections and TROPOMI aerosol index data.

The selected fire events were further refined using TROPOMI CO. During data exploration, we found that the TROPOMI Level 2 CO product could fail to provide valid CO retrievals for a few smoke pixels close to fire fronts over very large and intense fires. Thus, any selected fires with invalid CO observations were excluded. As a result, a total of 41 wildfires were finally extracted and they are mainly forest fires (figure 1(g)). For each selected fire, TROPOMI AI data were used to discriminate smoke plumes from the background, and CO observations inside the boundaries of a smoke plume were extracted as smoke CO (figures 1(e) and (f)). The smoke plume boundaries were then expanded outward

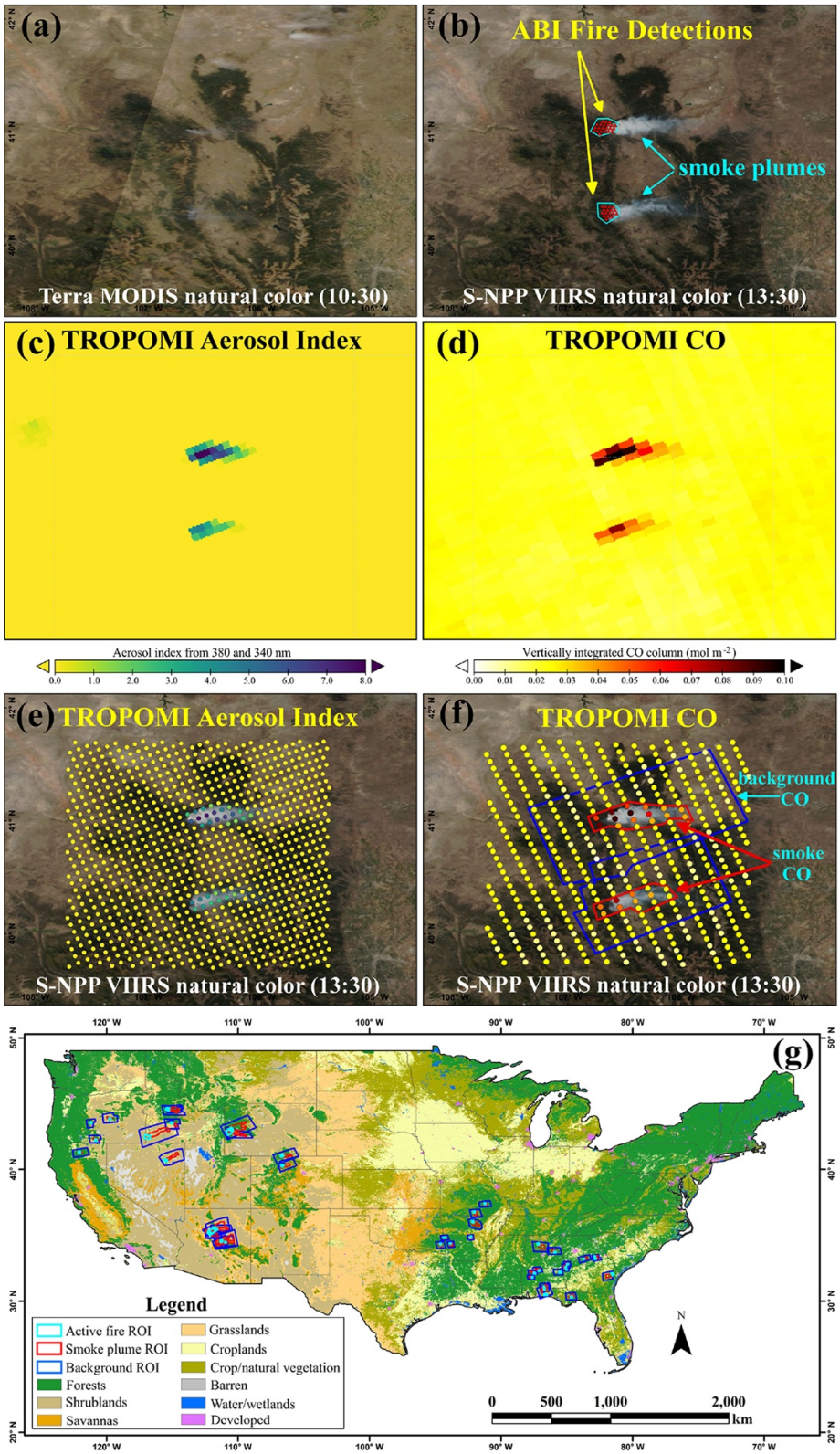

Figure 1. Selection of fire events with fresh smoke plumes. (a–d) illustrate an example of selecting two fires occurred at northern Colorado on 22 September 2018, and (g) shows the spatial distribution of the selected 41 fires across the CONUS during the period from July 2018 to October 2019. (a) Terra MODIS true-color composite observed at 10:30. (b) Two fire events confirmed by ABI active fire detections (red dots delineated by cyan polygons) overlain on S-NPP VIIRS true-color composite (observed at 13:30). (c–d) Aerosol index (based on 380/340 nm pair) and CO total column over the same region as in (a–b) observed by TROPOMI at 13:35. (e–f) Pixels of TROPOMI aerosol index and CO are represented by points at their centers for manually delineating smoke and non-smoke background pixels, which use the same legend as in (c–d), with the smoke plumes and non-smoke background delineated by red and blue polygons, respectively.

by a distance of at least three CO observations (~21 km = 7 km × 3 pixels), and the CO observations located at the region between smoke plume boundaries and the expanded boundaries were extracted as the background non-smoke CO (figure 1(d)). As the background pixels were not contaminated by clouds or smoke from other fires, the CO total column retrievals in the clear-sky observation conditions are able to well represent the true CO total columns (Borsdorff *et al* 2018a). Because the TROPOMI Level 2 CO data measure vertically integrated CO total column above land/water surface, TROPOMI CO over either smoke or background pixels also contains CO from other sources, including oxidation from methane and biogenic volatile organic compounds (VOCs), etc.

3.2. Comparison of the ABI FRP-based CO with TROPOMI CO

The total mass of fire smoke CO emissions was calculated using TROPOMI CO observations for each of the selected 41 fires. Because smoke plumes of the selected fires were just released within a few hours of the TROPOMI observation time, we assume that oxidation of the CO emissions during such a short period is negligible because atmospheric CO has a lifetime of about two months at middle latitudes (Khalil and Rasmussen 1990). Following the method used by (Heymann *et al* 2017), for each selected fire we first calculated background CO density by averaging the CO total column density of all the extracted non-smoke background CO pixels to account for non-fire contributions to the observed CO. Then the total mass of the fire-released CO emissions is calculated using TROPOMI CO observations as:

$$\boldsymbol{CO_t} = \sum_{i=1}^{n} \left[\left(\boldsymbol{\rho_{sm}^{i}} - \boldsymbol{\rho_{bg}} \right) \times \boldsymbol{A^{i}} \times \boldsymbol{M} \right] \quad (1)$$

where CO_t is the fire-released CO total mass (g) observed by TROPOMI, n is the number of TROPOMI CO pixels inside the associated smoke plume boundaries for a given fire, ρ_{sm}^{i} is the observed CO total column density (mole m^{-2}) of the ith TROPOMI smoke CO pixel, ρ_{bg} is the mean CO total column density (mole m^{-2}) of the non-smoke background pixels, A^{i} is pixel area (m^2) of the ith smoke CO pixel, and M is CO molecular mass (28.01 g mol^{-1}).

To examine the enhancement of CO over each fire smoke plume against the non-smoke background, we also calculated the dry-air CO total column mixing ratio (in units of parts per billion volume, abbreviated as ppbv) based on the TROPOMI CO total column density and the co-located surface pressure by following the method in Borsdorff *et al* (2018a). For the sake of simplicity, the CO column mixing ratio is referred to as the dry-air CO total column mixing ratio.

The total mass of the CO emissions was also calculated based on 5-min FRP retrievals from GOES-16 ABI using an FRE biomass combustion factor. (Wooster *et al* 2005) derived an FRE biomass combustion factor of 0.368 kg MJ^{-1} in a field experiment that has been commonly used to estimate regional-to-global biomass consumption and emissions (Zhang *et al* 2012, Roberts *et al* 2015). (Li *et al* 2018) reported an FRE combustion factor of 0.320 kg MJ^{-1} for the CONUS wildfires based on FRP from MODIS and GOES and the Landsat-based biomass consumption. For each selected fire, the total mass of the CO emissions was calculated using these two combustion factors separately:

$$\boldsymbol{CO_f} = \boldsymbol{FRE} \times \boldsymbol{B} \times \boldsymbol{F} \quad (2)$$

where CO_f is FRP-based CO total mass (g), FRE is the ABI FRP-based fire radiative energy (MJ), B is the FRE biomass combustion factor, and F is the CO emission factor (89 g kg^{-1} for temperate forests; Akagi *et al* 2011). By assuming that fire intensity is generally consistent within 5 min, the total radiative energy FRE is calculated using 5-min ABI FRP as:

$$\boldsymbol{FRE} = \sum_{k=1}^{q} \boldsymbol{FRE_k} = \sum_{k=1}^{q} \int_{t1}^{t2} \boldsymbol{FRP_k}(t)\, \boldsymbol{dt} \quad (3)$$

where, given a fire with a total number of q ABI fire detections, FRE_k is the fire radiative energy (MJ) observed at the kth ABI fire pixel during a burning period from $t1$ to $t2$. $t1$ is set as the observing time of the first valid GOES-16 ABI fire observation at the kth fire pixel and $t2$ is the TROPOMI overpass time. $FRP_k(t)$ is ABI FRP at observing time t ($t \in (t1, t2)$).

Then, the ABI FRP-based CO total mass estimates were compared statistically with the observed TROPOMI CO total mass estimates over the selected 41 fires using the ordinary least squares (OLS) regression.

Finally, the CO emission coefficient that converts FRP to the mass of the CO emissions was also derived from ABI FRE and TROPOMI CO observations using the following formula:

$$\boldsymbol{CO_t} = \boldsymbol{FRE} \times \boldsymbol{Ce} \quad (4)$$

where CO_t is the fire-released CO total mass (g) observed by TROPOMI, FRE is the ABI FRP-based fire radiative energy (MJ), and Ce is CO emissions coefficient (g MJ^{-1}). The CO emission coefficient was statistically calculated from 41 fire events using the OLS regression.

3.3. Comparison of the ABI FRP-based CO with the FINN, GFAS, and QFED CO

The CO emissions across the CONUS were estimated using ABI FRP and the derived CO emissions coefficient (Ce) at a grid resolution of 0.25° for the four months from June to September 2018. The result

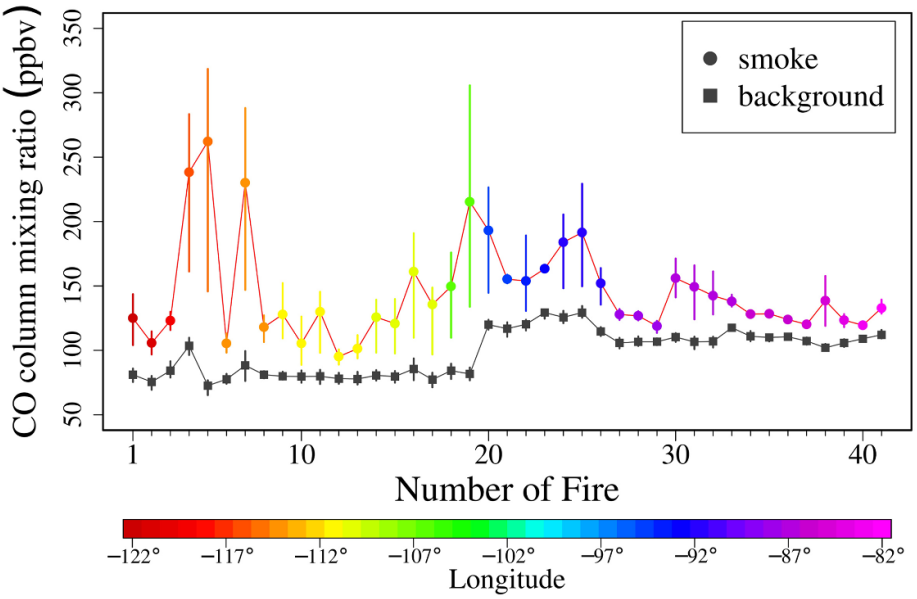

Figure 2. The TROPOMI CO column mixing ratios of the smoke plumes (colored cycles) and the non-smoke background (black squares) over the selected 41 fires. From left to right, fire samples are plotted along the longitude in the west-to-east direction, with colored circles and black squares representing the mean CO column mixing ratios of the smoke plumes and the background, respectively, and the error bars showing the CO column mixing ratio at percentiles 20% and 80% (error bars are not shown for a few eastern CONUS fires where smoke CO pixels are few).

was compared with the CO emissions from the FINN, GFAS, and QFED fire emissions inventories. The four months from June to September cover the typical fire season in the west CONUS where large wildfires are usually widespread (Zhang *et al* 2014b, Balch *et al* 2017). Specifically, for each ABI fire pixel, the daily FRE was first calculated by integrating the 5-min ABI FRP and then applied to calculate the daily CO emissions using the equation (4). The daily pixel-level CO emissions were further aggregated in a 0.25° grid and at an interval of one month. Finally, the ABI FRP-based monthly CO emissions were compared with the CO emissions from the FINN, GFAS, and QFED inventories.

4. Results and discussion

4.1. TROPOMI CO over smoke plumes and background

Smoke plumes show significantly higher CO concentration than the non-smoke background (figure 2). Over the selected 41 fires, the CO column mixing ratio of smoke plumes on average was 47 ppbv higher than that of the background, which represents a CO mixing ratio enhancement of 51%. The largest enhancements of 164% (135 ppbv) and 261% (190 ppbv) were seen over two fires in Idaho State. The CO enhancements were in similar ranges to the ground- and airborne-measured CO enhancement over wildfires in the western CONUS and North America boreal regions (Val Martín *et al* 2006, Ditas *et al* 2018). The mean CO mixing ratio enhancement was 79% in the western CONUS while it was 27% in the eastern CONUS. The large difference is partly due to the difference in the background CO between the two regions. The mean background CO column mixing ratio in the eastern CONUS (113 ppbv) is approximately 138% of that in the western CONUS (82 ppbv), which is consistent with the pattern based on long-term MOPITT CO observations (Deeter *et al* 2012, Jiang *et al* 2018). This is primarily attributed to the much larger contributions from anthropogenic and biogenic CO sources in the eastern CONUS (Hudman *et al* 2008, Jiang *et al* 2018).

4.2. The ABI FRP-based CO versus TROPOMI CO

The ABI FRP-based CO estimates agree well with the TROPOMI CO estimates (figure 3). Over the selected 41 fires, the total mass of the CO emissions estimated via the two FRE biomass combustion factors (equation (2)) was 0.001–6.78 Gg and 0.001–5.90 Gg, which has a similar magnitude to the TROPOMI CO based total mass: 0.015–6.21 Gg. The ABI FRP-based CO was significantly correlated to the observed TROPOMI CO ($R^2 = 0.94$, p-value < 0.001). When an FRE biomass combustion factor of 0.368 kg MJ^{-1} was applied, the FRP-based CO was overall slightly larger than TROPOMI CO by up to 18% at a 95% confidence interval, with an RMSE (root mean square error) of 0.3. For some relatively small fires, the FRP-based CO was smaller than TROPOMI CO, as indicated by the small negative bias. Similarly, the FRP-based CO via an FRE combustion factor of 0.320 kg MJ^{-1} was overall slightly smaller than TROPOMI CO by up to 13% at a 95% confidence interval, with an RMSE of 0.3. Although the ABI and TROPOMI sensors provide unprecedented spatiotemporal resolution observations of fires and smoke

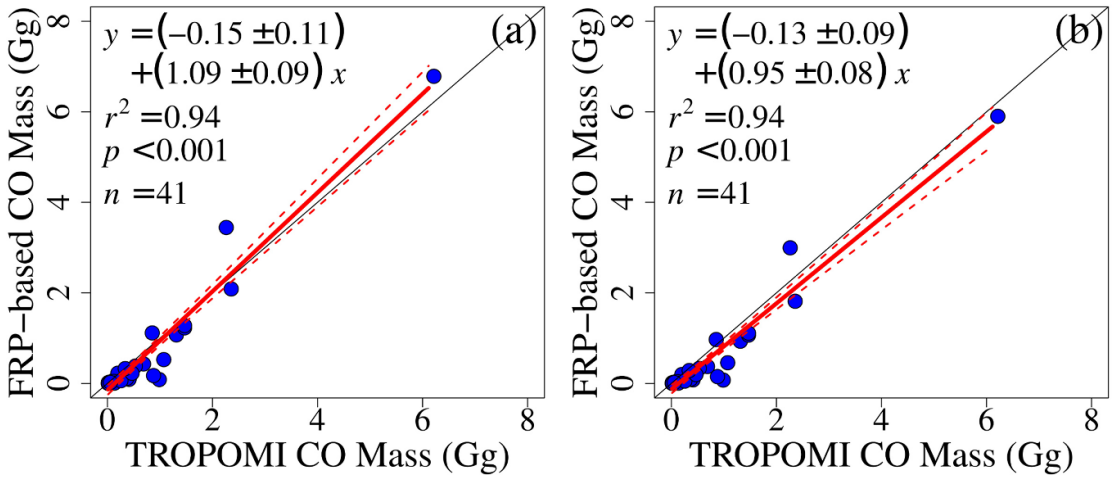

Figure 3. Comparisons of the observed TROPOMI CO and the ABI FRP-based CO estimated using two FRE biomass combustion factors: (a) 0.368 kg MJ^{-1} and (b) 0.320 kg MJ^{-1}. The red solid and dash lines represent the best-fit model and 95% confidence intervals, and the black solid line is 1:1 line.

emissions, the accuracy of the associated FRP and CO data could influence CO estimates for individual fires. However, the very good agreement between the ABI FRP-based CO and TROPOMI CO estimates over the 41 fires across the CONUS confirms the robustness of the FRP-based method for BBE estimation via FRE biomass combustion factors. The small difference (−13% – +18%) between the FRP-based CO and TROPOMI CO suggests that for the CONUS forest wildfires the uncertainty of the FRP-based BBE via the two FRE combustion factors is limited within 18%. This differs from the previous finding that BBE estimated via FRE combustion factor are largely underestimated and an increase of BBE by a factor of several times is needed to reduce the underestimation (Kaiser *et al* 2012, Darmenov and da Silva 2015).

4.3. Comparison of CO emission coefficient with other studies

Figure 4 shows a CO emission coefficient of 29.92 ± 2.39 g MJ^{-1} based on ABI FRE and TROPOMI CO over the selected 41 fires. The coefficient of determination indicates that 94% of the variation in CO could be explained by ABI FRE, which also implies that the derived CO emission coefficient can be used to calculate the CO emissions from FRP without bias and with limited uncertainties.

CO emission coefficient has been derived in several previous studies to directly estimate BBE using satellite-based FRP. In the published literature, CO emission coefficient has been derived directly by correlating lab-measured rate of the CO emissions to FRP (or mass of CO to FRE; Freeborn *et al* 2008) or indirectly inferring from the TPM (total particulate matters) emission coefficient based on the ratio of CO and TMP emission factors (Mota and Wooster 2018). Our CO emission coefficient is very close to the lab-based CO emission coefficient (33.71 g MJ^{-1}; Freeborn *et al* 2008). However, the CO emission coefficient converted from the AOD-derived TPM emission coefficient is much larger. (Mota and Wooster 2018) reported a CO emission coefficient of 142 g MJ^{-1} based on MODIS AOD and FRP from SEVIRI (Spinning Enhanced Visible and Infra-red Imager) in open-canopy forest fires in Africa. Similarly, (Ichoku and Ellison 2014) and (Lu *et al* 2019) separately showed a TPM emissions coefficient of 40 g MJ^{-1} and 21.73 g MJ^{-1} for the CONUS forest fires based on MODIS FRP and AOD data, which corresponds to a CO emission coefficient of 193 g MJ^{-1} and 105 g MJ^{-1}. One potential issue in deriving AOD-based CO emission coefficients is the uncertainties of the smoke mass extinction coefficient that converts AOD to TPM. The mass extinction coefficient varies between 2.22 and 7.6 m^2 g^{-1} as smoke ages, which has been discussed in (Mota and Wooster 2018). Moreover, previous studies also showed that the BBE estimated via the AOD-based coefficients is larger than BBE estimates calculated via FRE biomass combustion factor by a factor of several times (Zhang *et al* 2014a, Li *et al* 2019, Carter *et al* 2020). As a result, it is reasonable to deduce that combining ABI FRE and TROPOMI CO could provide a much reliable CO emission coefficient.

4.4. The ABI FRP-based CO emissions across the CONUS

Figure 5 shows the spatial patterns of the ABI FRP-based monthly CO emissions across the CONUS from June to September 2018. During this period, fires occurred in most regions of the CONUS but the fire-released CO emissions varied significantly spatially. Fires in the western CONUS accounted for 82%, 92%, 95%, and 93% of the monthly total CO emissions across the CONUS in the four months, respectively. In the same period, however, fires in the eastern CONUS released a relatively very limited amount of the CO emissions, which were

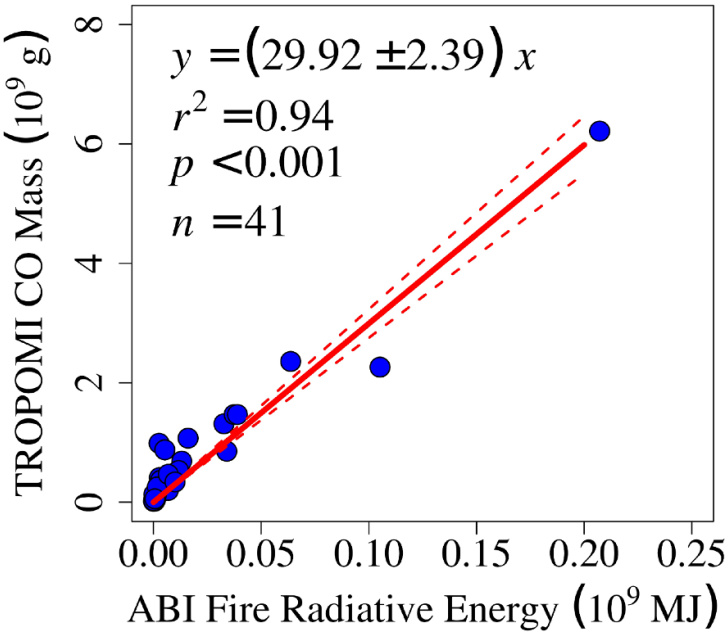

Figure 4. The CO emission coefficient based on ABI FRE and TROPOMI CO. The red solid and dash lines are the best-fit model and 95% confidence intervals.

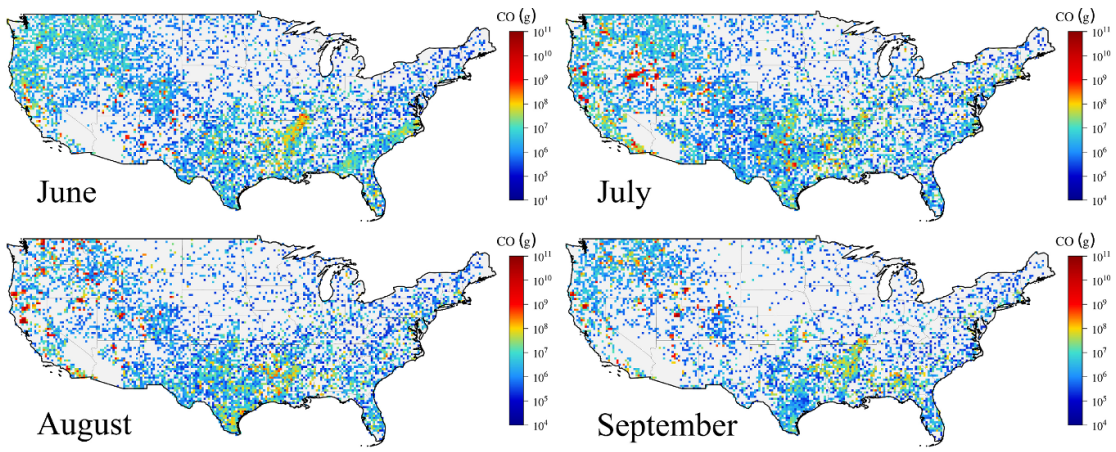

Figure 5. The ABI FRP-based monthly CO emissions in a 0.25° grid across the CONUS from June to September 2018.

mainly contributed by fires across the southeastern CONUS. This is consistent with the previous finding that the majority portion of the CONUS emissions is from fires across the western CONUS during the summer months (Urbanski *et al* 2018, Li *et al* 2019).

The ABI FRP-based CO emissions provide a good reference for evaluating the CO emissions from the existing fire emissions inventories. Figure 6 shows the monthly total CO emissions based on ABI FRP and from the FINN, GFAS, and QFED emissions inventories across the CONUS. In the four months from June to September, the ABI FRP-based monthly CO emissions were 294 (±23) Gg, 702 (±56) Gg, 934 (±75) Gg, and 455 (±36) Gg, respectively. In comparison with the three inventories, the ABI FRP-based monthly CO emissions on average were very similar to the FINN and GFAS CO, with a mean difference of less than 13%, but differed from the QFED CO by a factor of approximately four. Although the mean of the ABI FRP-based monthly CO emissions (596 Gg) was comparable with that of the GFAS CO (670 Gg), the ABI FRP-based CO and the FINN and QFED CO peaked in August while the GFAS CO peaked in September and was the smallest in August among all the four CO datasets. Further, previously published studies also found that the QFED emissions were much larger than the other emissions inventories across the CONUS and other regions, with a difference of 2–6 times (Li *et al* 2019, Carter *et al* 2020, Pan *et al* 2020). The large discrepancies are most likely associated with the fact that the QFED emissions are

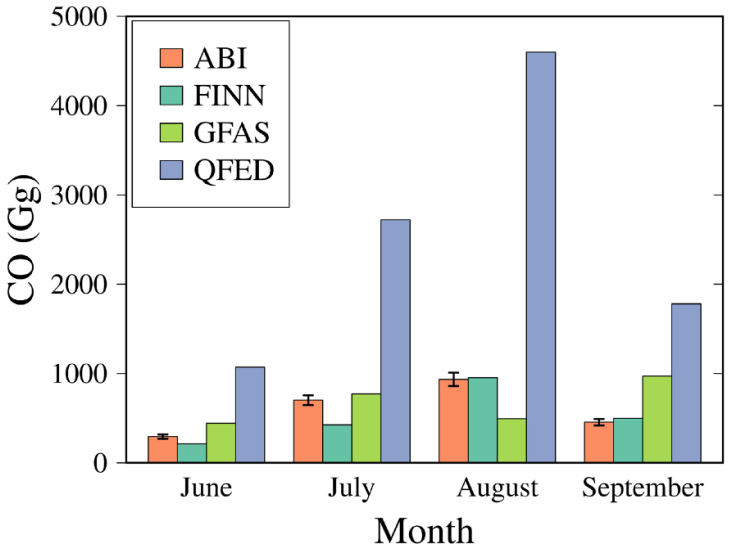

Figure 6. Monthly CO emissions based on the ABI FRP and from the FINN, GFAS, and QFED emissions inventories. The error bars represent one standard deviation of the ABI FRP-based CO emissions.

significantly enlarged by the MODIS AOD based scaling factors (Carter *et al* 2020).

Potential uncertainties in the ABI FRP-based CO emissions estimates could arise from the omission errors in the ABI fire detection and the application of the single CO emission coefficient. First, the GOES-16 ABI sensor could miss very small and/or cool fires at large view angles in the northwestern CONUS because of the decrease in pixel resolution although its high temporal resolution significantly improves the fire detection capability (Li *et al* 2020). Luckily, the portion of small fires in the northwestern CONUS is much smaller than that in the southeastern CONUS (Randerson *et al* 2012) where the ABI sensor has a fire detection capability comparable to the VIIRS sensor (Li *et al* 2020). Thus, the uncertainty of the ABI FRP-based CO due to the omission errors of the ABI fire detections could be relatively small. Second, the CO emissions across the CONUS in this comparison were calculated using the single CO emission coefficient that was derived based on the TROPOMI CO over mostly forest fires (figure 4). For other types of fires (e.g. agricultural burnings), the CO emission coefficient could be different, which could introduce certain uncertainties in the CO emissions estimates. However, this effect could be limited in this comparison because fires, especially large forest wildfires, in the western CONUS contributed to the majority portion (82% in June and >90% in the following three months) of the CO emissions across the CONUS.

5. Conclusions

Accurate and timely estimation of BBE is crucial for understanding the role of biomass burning in the atmosphere and biosphere. Satellite-based FRP provides an effective way to estimate fire emissions at a regional-to-global scale. Because of the lack of direct and good-quality observations of BBE, current BBE estimates from satellite data are generally not fully validated. This study proposed a new algorithm to make a reliable and applicable evaluation of fire emissions estimates, which is to select fresh fire events detected by TROPOMI. As a result, this study evaluated the FRP-based method for fire emissions estimation using the 7-km Sentinel-5P TROPOMI CO and 2-km GOES-16 ABI FRP observations every 5 min over 41 fresh fires occurred during July 2018—October 2019 across the CONUS. The results show that smoke plumes on average enhance CO emissions by 51% compared with the non-smoke background over the 41 fires, and the ABI FRP-based CO estimates are significantly correlated to the TROPOMI CO with an overall difference of 13–18%. This result confirms that fire emissions can be well estimated from the FRE biomass combustion factors. Additionally, based on ABI FRE and TROPOMI CO, this study reports a CO emission coefficient of 29.92 $\pm$ 2.39 g MJ^{-1}, which is very close to the one derived in the lab experiment. This coefficient, combined with ABI FRP, was further used to estimate the CO emissions across the CONUS during the 2018 summer months. The ABI FRP-based CO emissions provide a direct reference for evaluating the existing BBE inventories, which helps us understand the large discrepancies among the existing BBE inventories. Mitigating the uncertainty in BBE estimation could significantly improve the predictions of air quality and radiative effect(Vongruang *et al* 2017, Carter *et al* 2020). The algorithm proposed in this study is expected to be expanded to other fire-prone regions where high temporal resolution FRP observations from the latest geostationary sensors (e.g. ABI, SEVIRI, and the

Advanced Himawari Imager) are available. The high-spatiotemporal-resolution observations of the fire-released atmospheric pollutants from the advanced instruments like the Geostationary Environment Monitoring Spectrometer (GEMS; Kim *et al* 2020) and the Tropospheric Emissions: Monitoring of Pollution (TEMPO; Zoogman *et al* 2017) will make it possible to examine the diurnal variation of emissions coefficients, which could further improve the accuracy of BBE estimation and advance our understanding of the effects of BBE on climate, weather and environmental conditions, and human health.

Data availability statement

All data that support the findings of this study are included within the article (and any supplementary information files).

Acknowledgments

This study is supported by NOAA contract NA14NES4320003 and NASA contract 80NSSC18K0235. We thank NOAA for providing GOES-16 ABI active fire data and Copernicus for providing Sentinel-5P TROPOMI CO data. The ABI active fire data and TROPOMI CO and aerosol index data are freely available for public access at NOAA CLASS (https://www.avl.class.noaa.gov/; last accessed on 3 April 2020) and the Copernicus Sentinel-5P pre-operations data hub (https://s5phub.copernicus.eu//; last accessed on 3 April 2020). We also thank the groups of the FINN (http://bai.acom.ucar.edu/Data/fire/; last accessed on 18 May 2020), GFAS (https://apps.ecmwf.int/datasets/data/cams-gfas/; last accessed on 18 May 2020), and QFED (https://portal.nccs.nasa.gov/datashare/iesa/aerosol/emissions/QFED/v2.5r1/0.1/; last access on 18 May 2020) for making the products available. We thank two anonymous reviewers for their constructive comments that improved this work. The views, opinions, and findings contained in this manuscript are those of the author(s) and should not be interpreted as an official NOAA or U.S. government position, policy, or decision.

ORCID iDs

Fangjun Li https://orcid.org/0000-0003-4267-089X
Xiaoyang Zhang https://orcid.org/0000-0001-8456-0547

References

Akagi S K, Yokelson R J, Wiedinmyer C, Alvarado M J, Reid J S, Karl T, Crounse J D and Wennberg P O 2011 Emission factors for open and domestic biomass burning for use in atmospheric models *Atmos. Chem. Phys.* **11** 4039–72

Apituley A, Pedergnana M, Sneep M, Veefkind J P, Loyola D and Stein Zweers D 2018 Sentinel-5 precursor/TROPOMI level 2 product user manual UV aerosol index (https://sentinel.esa.int/documents/247904/2474726/Sentinel-5P-Level-2-Product-User-Manual-Aerosol-Index-product) (Accessed: 1 April 2020)

Balch J K, Bradley B A, Abatzoglou J T, Nagy R C, Fusco E J and Mahood A L 2017 Human-started wildfires expand the fire niche across the United States *Proc. Natl Acad. Sci.* **114** 2946–51

Borsdorff T *et al* 2018a Mapping carbon monoxide pollution from space down to city scales with daily global coverage *Atmos. Meas. Tech.* **11** 5507–18

Borsdorff T, Aan de Brugh J, Hu H, Aben I, Hasekamp O and Landgraf J 2018b Measuring carbon monoxide with TROPOMI: first results and a comparison with ECMWF-IFS analysis data *Geophys. Res. Lett.* **45** 2826–32

Borsdorff T, Andrasec J, Aan de Brugh J, Hu H, Aben I and Landgraf J 2018c Detection of carbon monoxide pollution from cities and wildfires on regional and urban scales: the benefit of CO column retrievals from SCIAMACHY 2.3 μm measurements under cloudy conditions *Atmos. Meas. Tech.* **11** 2553–65

Carter T S *et al* 2020 How emissions uncertainty influences the distribution and radiative impacts of smoke from fires in North America *Atmos. Chem. Phys.* **20** 2073–97

Curci G *et al* 2015 Uncertainties of simulated aerosol optical properties induced by assumptions on aerosol physical and chemical properties: an AQMEII-2 perspective *Atmos. Environ.* **115** 541–52

Darmenov A S and da Silva A 2015 The Quick Fire Emissions Dataset (QFED): Documentation of versions 2.1, 2.2 and 2.4Rep. TM–2015–104606 pp212 NASA (https://ntrs.nasa.gov/archive/nasa/casi.ntrs.nasa.gov/20180005253.pdf)

Das S, Harshvardhan H, Bian H, Chin M, Curci G, Protonotariou A P, Mielonen T, Zhang K, Wang H and Liu X 2017 Biomass burning aerosol transport and vertical distribution over the South African-Atlantic region *J. Geophys. Res. Atmos.* **122** 6391–415

Ditas J *et al* 2018 Strong impact of wildfires on the abundance and aging of black carbon in the lowermost stratosphere *Proc. Natl Acad. Sci.* **115** E11595-E11603

Deeter M N, Worden H M, Edwards D P, Gille J C and Andrews A E 2012 Evaluation of MOPITT retrievals of lower-tropospheric carbon monoxide over the United States *J. Geophys. Res. Atmos.* **117** 4399

Dekker I N, Houweling S, Pandey S, Krol M, Röckmann T, Borsdorff T, Landgraf J and Aben I 2019 What caused the extreme CO concentrations during the 2017 high-pollution episode in India? *Atmos. Chem. Phys.* **19** 3433–45

Duncan B N, Logan J A, Bey I, Megretskaia I A, Yantosca R M, Novelli P C, Jones N B and Rinsland C P 2007 Global budget of CO, 1988–1997: source estimates and validation with a global model *J. Geophys. Res. Atmos.* **112** D22301

Freeborn P H, Wooster M J, Hao W M, Ryan C A, Nordgren B L, Baker S P and Ichoku C 2008 Relationships between energy release, fuel mass loss, and trace gas and aerosol emissions during laboratory biomass fires *J. Geophys. Res. Atmos.* **113** D01301

Hall J V, Zhang R, Schroeder W, Huang C and Giglio L 2019 Validation of GOES-16 ABI and MSG SEVIRI active fire products *Int. J. Appl. Earth Obs. Geoinf.* **83** 101928

Heald C L, Jacob D J, Jones D B A, Palmer P I, Logan J A, Streets D G, Sachse G W, Gille J C, Hoffman R N and Nehrkorn T 2004 Comparative inverse analysis of satellite (MOPITT) and aircraft (TRACE-P) observations to estimate Asian sources of carbon monoxide *J. Geophys. Res. Atmos.* **109** D23306

Heymann J, Reuter M, Buchwitz M, Schneising O, Bovensmann H, Burrows J P, Massart S, Kaiser J W and Crisp D 2017 CO2 emission of Indonesian fires in 2015 estimated from satellite-derived atmospheric CO2 concentrations *Geophys. Res. Lett.* **44** 1537–44

Hudman R C, Murray L T, Jacob D J, Millet D B, Turquety S, Wu S, Blake D R, Goldstein A H, Holloway J and Sachse G W 2008 Biogenic versus anthropogenic sources of CO in the United States *Geophys. Res. Lett.* **35** L04801

Huijnen V, Wooster M J, Kaiser J W, Gaveau D L A, Flemming J, Parrington M, Inness A, Murdiyarso D, Main B and van Weele M 2016 Fire carbon emissions over maritime southeast Asia in 2015 largest since 1997 *Sci. Rep.* **6** 26886

Ichoku C and Ellison L 2014 Global top-down smoke-aerosol emissions estimation using satellite fire radiative power measurements *Atmos. Chem. Phys.* **14** 6643–67

Ichoku C and Kaufman Y J 2005 A method to derive smoke emission rates from MODIS fire radiative energy measurements *IEEE Trans. Geosci. Remote Sens.* **43** 2636–49

Ichoku C, Martins J V, Kaufman Y J, Wooster M J, Freeborn P H, Hao W M, Baker S, Ryan C A and Nordgren B L 2008 Laboratory investigation of fire radiative energy and smoke aerosol emissions *J. Geophys. Res. Atmos.* **113** D14S09

Jiang Z, Jones D B A, Kopacz M, Liu J, Henze D K and Heald C 2011 Quantifying the impact of model errors on top-down estimates of carbon monoxide emissions using satellite observations *J. Geophys. Res. Atmos.* **116** D15306

Jiang Z, Jones D B A, Worden H M, Deeter M N, Henze D K, Worden J, Bowman K W, Brenninkmeijer C A M and Schuck T J 2013 Impact of model errors in convective transport on CO source estimates inferred from MOPITT CO retrievals *J. Geophys. Res. Atmos.* **118** 2073–83

Jiang Z *et al* 2018 Unexpected slowdown of US pollutant emission reduction in the past decade *Proc. Natl Acad. Sci.* **115** 5099–104

Jiang Z, Worden J R, Worden H, Deeter M, Jones D B A, Arellano A F and Henze D K 2017 A 15-year record of CO emissions constrained by MOPITT CO observations *Atmos. Chem. Phys.* **17** 4565–83

Johnston F H, Henderson S B, Chen Y, Randerson J T, Marlier M, Defries R S, Kinney P, Bowman D M and Brauer M 2012 Estimated global mortality attributable to smoke from landscape fires *Environ. Health Perspect.* **120** 695–701

Jones D B A, Bowman K W, Logan J A, Heald C L, Liu J, Luo M, Worden J and Drummond J 2009 The zonal structure of tropical O3 and CO as observed by the Tropospheric Emission Spectrometer in November 2004 – part 1: inverse modeling of CO emissions *Atmos. Chem. Phys.* **9** 3547–62

Kaiser J W *et al* 2012 Biomass burning emissions estimated with a global fire assimilation system based on observed fire radiative power *Biogeosciences* **9** 527–54

Khalil M A K and Rasmussen R A 1990 The global cycle of carbon monoxide: trends and mass balance *Chemosphere* **20** 227–42

Kim J *et al* 2020 New era of air quality monitoring from space: geostationary environment monitoring spectrometer (GEMS) *Bull. Am. Meteorol. Soc.* **101** E1-E22

Kopacz M *et al* 2010 Global estimates of CO sources with high resolution by adjoint inversion of multiple satellite datasets (MOPITT, AIRS, SCIAMACHY, TES) *Atmos. Chem. Phys.* **10** 855–76

Kremens R L, Dickinson M B and Bova A S 2012 Radiant flux density, energy density and fuel consumption in mixed-oak forest surface fires *Int. J. Wildland Fire* **21** 722–30

Landgraf J, Aan de Brugh J, Scheepmaker R, Borsdorff T, Hu H, Houweling S, Butz A, Aben I and Hasekamp O 2016 Carbon monoxide total column retrievals from TROPOMI shortwave infrared measurements *Atmos. Meas. Tech.* **9** 4955–75

Li F, Zhang X, Kondragunta S and Roy D P 2018 Investigation of the fire radiative energy biomass combustion coefficient: a comparison of polar and geostationary satellite retrievals over the conterminous United States *J. Geophys. Res. Biogeosci.* **123** 722–39

Li F, Zhang X, Kondragunta S, Schmidt C C and Holmes C D 2020 A preliminary evaluation of GOES-16 active fire product using landsat-8 and VIIRS active fire data, and ground-based prescribed fire records *Remote Sens. Environ.* **237** 111600

Li F, Zhang X, Roy D P and Kondragunta S 2019 Estimation of biomass-burning emissions by fusing the fire radiative power retrievals from polar-orbiting and geostationary satellites across the conterminous United States *Atmos. Environ.* **211** 274–87

Lu X, Zhang X, Li F and Cochrane M A 2019 Investigating smoke aerosol emission coefficients using MODIS active fire and aerosol products — a case study in the CONUS and indonesia *J. Geophys. Res. Biogeosci.* **124** 1413–29

Mota B and Wooster M J 2018 A new top-down approach for directly estimating biomass burning emissions and fuel consumption rates and totals from geostationary satellite fire radiative power (FRP) *Remote Sens. Environ.* **206** 45–62

Pan X *et al* 2020 Six global biomass burning emission datasets: intercomparison and application in one global aerosol model *Atmos. Chem. Phys.* **20** 969–94

Pechony O, Shindell D T and Faluvegi G 2013 Direct top-down estimates of biomass burning CO emissions using TES and MOPITT versus bottom-up GFED inventory *J. Geophys. Res. Atmos.* **118** 8054–66

Randerson J T, Chen Y, van der Werf G R, Rogers B M and Morton D C 2012 Global burned area and biomass burning emissions from small fires *J. Geophys. Res. Biogeosci.* **117** G04012

Roberts G, Wooster M J, Xu W, Freeborn P H, Morcrette J J, Jones L, Benedetti A, Jiangping H, Fisher D and Kaiser J W 2015 LSA SAF meteosat FRP products – part 2: evaluation and demonstration for use in the copernicus atmosphere monitoring service (CAMS) *Atmos. Chem. Phys.* **15** 13241–67

Roteta E, Bastarrika A, Padilla M, Storm T and Chuvieco E 2019 Development of a Sentinel-2 burned area algorithm: generation of a small fire database for sub-Saharan Africa *Remote Sens. Environ.* **222** 1–17

Roy D P, Huang H, Boschetti L, Giglio L, Yan L, Zhang H H and Li Z 2019 Landsat-8 and sentinel-2 burned area mapping - A combined sensor multi-temporal change detection approach *Remote Sens. Environ.* **231** 111254

Schmidt C C, Hoffman J and Prins E M 2013 GOES-R advanced baseline imager (ABI) algorithm theoretical basis document for fire/hot spot characterization version 2.6 NOAA NESDIS STAR pp 1–97 (https://www.star.nesdis.noaa.gov/goesr/documents/ATBDs/Baseline/ATBD_GOES-R_FIRE_v2.6_Oct2013.pdf) (Accessed: 1 April 2020)

Seiler W and Crutzen P 1980 Estimates of gross and net fluxes of carbon between the biosphere and the atmosphere from biomass burning *Clim. Change* **2** 207–47

Shindell D T *et al* 2006 Multimodel simulations of carbon monoxide: comparison with observations and projected near-future changes *J. Geophys. Res. Atmos.* **111** D19306

Tosca M G, Randerson J T and Zender C S 2013 Global impact of smoke aerosols from landscape fires on climate and the Hadley circulation *Atmos. Chem. Phys.* **13** 5227–41

Urbanski S P, Reeves M C, Corley R E, Silverstein R P and Hao W M 2018 Contiguous United States wildland fire emission estimates during 2003–2015 *Earth Syst. Sci. Data.* **10** 2241–74

Val Martín M, Honrath R E, Owen R C, Pfister G, Fialho P and Barata F 2006 Significant enhancements of nitrogen oxides, black carbon, and ozone in the North Atlantic lower free troposphere resulting from North American boreal wildfires *J. Geophys. Res. Atmos.* **111** D23S60

van der Werf G R *et al* 2017 Global fire emissions estimates during 1997–2016 *Earth Syst. Sci. Data.* **9** 697–720

Veefkind J P et al 2012 TROPOMI on the ESA sentinel-5 precursor: A GMES mission for global observations of the atmospheric composition for climate, air quality and ozone layer applications *Remote Sens. Environ.* **120** 70–83

Vermote E, Ellicott E, Dubovik O, Lapyonok T, Chin M, Giglio L and Roberts G J 2009 An approach to estimate global biomass burning emissions of organic and black carbon from MODIS fire radiative power *J. Geophys. Res. Atmos.* **114** D18205

Vidot J, Landgraf J, Hasekamp O P, Butz A, Galli A, Tol P and Aben I 2012 Carbon monoxide from shortwave infrared reflectance measurements: A new retrieval approach for clear sky and partially cloudy atmospheres *Remote Sens. Environ.* **120** 255–66

Vongruang P, Wongwises P and Pimonsree S 2017 Assessment of fire emission inventories for simulating particulate matter in upper Southeast Asia using WRF-CMAQ *Atmos. Pollut. Res.* **8** 921–9

Wiedinmyer C, Akagi S K, Yokelson R J, Emmons L K, Al-Saadi J A, Orlando J J and Soja A J 2011 The fire inventory from NCAR (FINN): a high resolution global model to estimate the emissions from open burning *Geosci. Model Dev.* **4** 625–41

Wooster M J, Roberts G, Perry G L W and Kaufman Y J 2005 Retrieval of biomass combustion rates and totals from fire radiative power observations: FRP derivation and calibration relationships between biomass consumption and fire radiative energy release *J. Geophys. Res. Atmos.* **110** D24311

Zhang F, Wang J, Ichoku C, Hyer E J, Yang Z, Ge C, Su S, Zhang X, Kondragunta S and Kaiser J W 2014a Sensitivity of mesoscale modeling of smoke direct radiative effect to the emission inventory: a case study in northern sub-Saharan African region *Environ. Res. Lett.* **9** 075002

Zhang X, Kondragunta S, Ram J, Schmidt C and Huang H-C 2012 Near-real-time global biomass burning emissions product from geostationary satellite constellation *J. Geophys. Res. Atmos.* **117** D14201

Zhang X, Kondragunta S and Roy D P 2014b Interannual variation in biomass burning and fire seasonality derived from geostationary satellite data across the contiguous United States from 1995 to 2011 *J. Geophys. Res. Biogeosci.* **119** 2013JG002518

Zoogman P et al 2017 Tropospheric emissions: monitoring of pollution (TEMPO) *J. Quant. Spectrosc. Radiat. Transfer.* **186** 17–39